Dynamic In-Situ Experimentation on Nanomaterials at the Atomic Scale

*Tao Xu and Litao Sun**

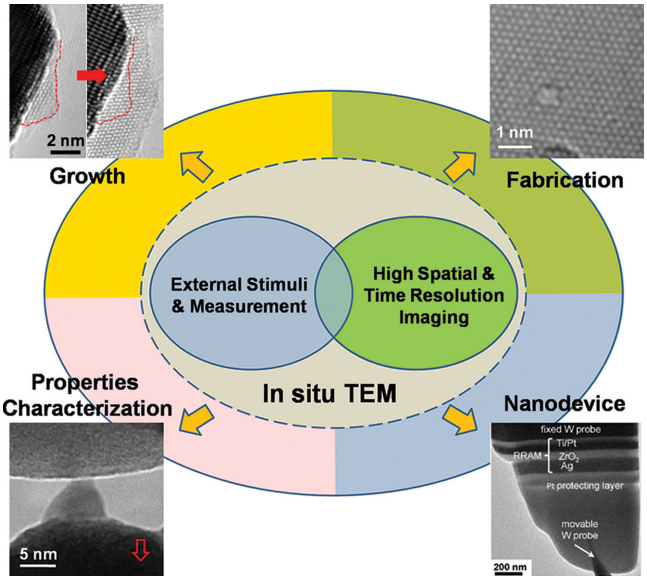

From the Contents

With the development of in situ techniques inside transmission electron microscopes (TEMs), external fields and probes can be applied to the specimen. This development transforms the TEM specimen chamber into a nanolab, in which reactions, structures, and properties can be activated or altered at the nanoscale, and all processes can be simultaneously recorded in real time with atomic resolution. Consequently, the capabilities of TEM are extended beyond static structural characterization to the dynamic observation of the changes in specimen structures or properties in response to environmental stimuli. This extension introduces new possibilities for understanding the relationships between structures, unique properties, and functions of nanomaterials at the atomic scale. Based on the idea of setting up a nanolab inside a TEM, tactics for design of in situ experiments inside the machine, as well as corresponding examples in nanomaterial research, including in situ growth, nanofabrication with atomic precision, in situ property characterization, and nanodevice construction are presented.

www.MaterialsViews.com

1. Introduction

Nanomaterials and nanostructures have received considerable interest because of their unique properties, which are significantly different from the properties of bulk materials. Many kinds of nanomaterials have been applied to, or have shown great potential in applications for, the efficient use of natural resources, efficient energy conversion, and efficient environmental protection, thereby indicating their relevance to a sustainable future. However, the relationship among the structures, unique properties, and functions of a nanosystem is not well understood. Characterization of structure or property responses to stimuli from the surrounding environment at the nanometer or atomic scale would play a crucial role in understanding the structure–property–function correlation and developing new and improved nanostructures for versatile applications.

Transmission electron microscopy (TEM), which has been significantly enhanced by recent advancements, has become a powerful and indispensable tool for nanomaterial characterization with atomic resolution. However, conventional TEM has focused only on stable structures in vacuum because of technical feasibility. The dynamic state of nanomaterials "in operation" cannot always be inferred from comparison of the beginning and ending state of the materials. Thus, meeting the increasing demands of nanomaterials research, in which the evolution of materials in dynamic environments is key information, is difficult.

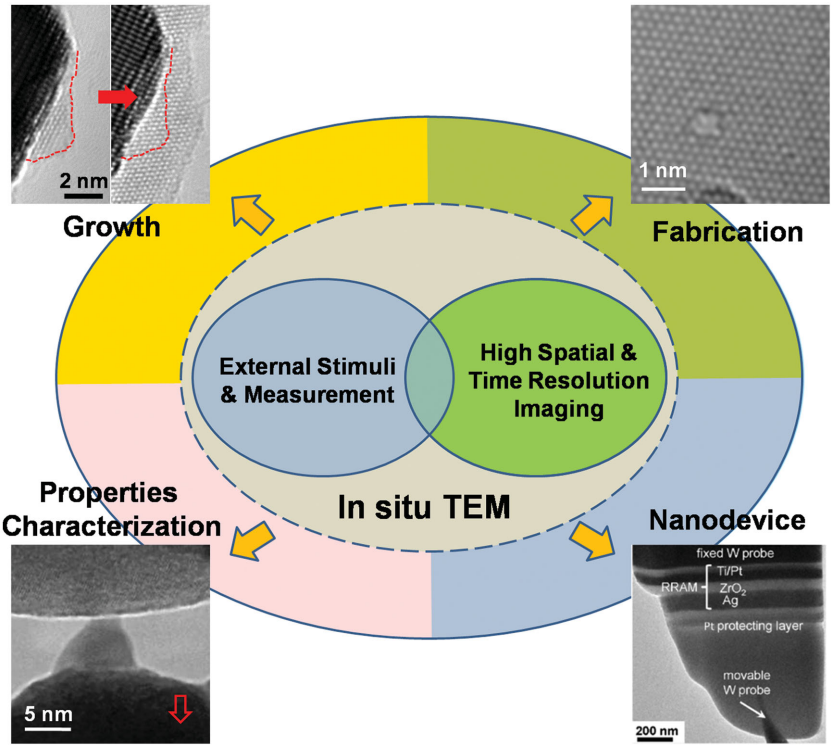

Figure 1. Schematic diagram showing the application of in situ TEM in studies on nanomaterials, including dynamic observation of growth, fabrication with atomic precision, property characterization (reproduced with permission.[147] Copyright 2014, Macmillan Publishing), and nanodevice reconstruction (reproduced with permission[37]) inside the TEM. In situ TEM will play a crucial role in clarifying the structure–property–function correlation of materials.

In situ TEM provides great opportunities to dynamically characterize the structures, chemical compositions and properties of materials under various external stimuli—including electron irradiation, thermal excitation, mechanical force, optical excitation, electric and magnetic field—in real time. The main difference of in situ TEM from conventional TEM is that an additional external field can be directly applied to the specimen during observation of its structure. The electron beam is the easiest and most direct stimulus inside the TEM. Electron irradiation is inevitable, because the imaging electrons will always interact with specimen atoms.[1–5] Hence, in situ electron irradiation experiments were initially studied, including electron irradiation-induced growth/phase transitions and nanofabrication[6–13] (**Figure 1**). The subsequent development of environmental cells allowing handling of gas or liquid in the specimen chamber of TEM brought about an era of monitoring dynamic processes—such as catalytic nanocrystal growth in gas[14–19] and colloidal nanoparticle growth in liquid[20–24]—under a variety of reaction conditions at and below nanoscale . It is crucial to mimic real world conditions inside the TEM chambers so that revolutionary insights and understanding of material growth are possible. To further apply additional external fields to the specimen area, a variety of special TEM specimen holders have been developed and improved.[25–27] Depending on which external field is to be applied, the special holder can be designed by adding a corresponding action element at the tip of a TEM holder. For example, an in situ heating holder can be realized by placing a heating element into the TEM holder (thermal radiation is used to heat the specimen generally), which can reveal materials' responses to high temperatures, even beyond 1600 K.[26,28] Conversely, low temperatures, even below 10 K, can be reached by cooling with liquid nitrogen or liquid helium,allowing in situ cooling experiments to study the materials' properties at low temperatures. The development of mechanical and electrical holders that enable quantitative measurements of mechanical forces in the nanonewton range, and currents in the nanoampere range, respectively, has shed light on the relationship between

T. Xu, Prof. L. Sun
SEU-FEI Nano-Pico Center
Key Lab of MEMS of Ministry of Education
Southeast University
Nanjing 210096, PR China
E-mail: slt@seu.edu.cn

DOI: 10.1002/smll.201403236

atomic structures and mechanical/electrical properties. The capability of applying external fields or forces to TEM specimens transforms the TEM specimen chamber into a miniaturized laboratory, in which chemical reactions, structures, or physical properties can be activated or altered at micrometer to nanometer scales. On the other hand, the development of ultrafast imaging—at picosecond and even femtosecond speeds—provides the opportunity to discover new phenomena in ultrashort time scales inside the TEM,[29–33] with the potential to decipher fundamentaldetails within complex structures. Furthermore, the development of the holder design and the design of the specimens ensured the workability of the nanodevice inside the TEM,[34–38] thereby providing further insight into the property–function relationship, resulting in the efficient use of natural resources.

In this review, we focus on the nanoscale and atomic scale visualization of structural evolution in functional nanomaterials and nanodevices under (near) operational or environmental conditions. The technical directions of setting up in situ experiments in TEM, as shown in Figure 1, are demonstrated and discussed with corresponding examples, such as in situ growth, nanofabrication at atomic resolution, in situ property characterization, and nanodevice construction.

Tao Xu is a PhD student in the School of Electronic Science and Engineering at Southeast University. He obtained his BE degree in 2009 from the Southeast University, China. His research interests focus mainly on in situ experimentation inside the transmission electron microscope, and 2D materials.

Litao Sun is currently a distinguished professor at Southeast University, China. He received his PhD from the Shanghai Institute of Applied Physics, Chinese Academy of Sciences, followed by postdoctoral research at University of Mainz, Germany and a visiting professorship at the University of Strasbourg, France. His current research interests include in situ experimentation inside the electron microscope, graphene and related 2D materials, new phenomena from sub-10 nm nanoparticles/nanowires, and applications of nanomaterials in environment, renewable energy and nanoelectromechanical systems.

2. In Situ Growth of Nanomaterials

Understanding the processes of material growth at nanoscale is important for designing nanostructured materials and for developing materials with novel properties. Given its capability to record structural and compositional changes as a function of time, TEM provides deep insights into growth processes, based on quantitative thermodynamic and kinetic data. However, the study of in situ growth inside the machine remains difficult.

The most significant problem is the source material. In conventional TEM, obtaining high spatial resolution involves exposing specimens to high vacuum (10^{-6} Torr or higher), in which liquid and gas precursors are hardly preserved. This condition limits the study of in situ growth in TEM. One solution is to use a solid source. Inside the TEM, the imaging electrons will transfer energy to the specimen on passing through the specimen, which may knock the specimen atoms away from their lattice positions.[1,2] The knocked atoms can migrate on the surface, or inside the bulk, and act as the source of growth. An example showing growth inside the TEM is the healing of nanopores embedded in solid membranes under electron irradiation.[39–42] The knocked atoms will reconstruct after their migration to the pore periphery to low surface free energy, thereby leading to the shrinkage and even disappearance of the pore. On the other hand, with the development of environmental cells, gases and liquids can be introduced into the specimen area while the other parts of the microscope column remain in high vacuum, providing an opportunity to study material growth at the atomic scale inside TEM chambers, under environments similar to real world conditions.

2.1. Solid-Source Growth Under Electron Irradiation

As mentioned above, electron beams, which can transfer energy to the specimen, play an important role in solid-source growth inside the TEM. Electron irradiation is a complex process, including many effects such as knock-on, sputtering, heating, ionization, electrostatic charging and so on.[2] When the transferred energy from the incident electrons is larger than the threshold energy for displacement, the specimen atoms will be displaced within the bulk and sputtered from the surface. The knocked atoms, especially those still adsorbed on the surface, are easily diffused after obtaining enough energy from the incident electrons. The rate of beam-induced motion is even predicted to exceed that of room temperature thermal emotion when surface diffusion energy of the adatom is greater than 0.5 eV.[43] On the other hand, the temperature rise in the specimen due to electron irradiation inside the TEM may range from a few to several hundred degrees (depending on the materials, beam current, and some other factors), which is sometimes high enough to cause visible phase transformations.[10] All these effects play important roles in nanocrystal growth inside the TEM. Furthermore, external thermal excitation can also accelerate the migration and reconstruction of adatoms or defects, thereby promoting the formation of new phases or structures.[3,5,44,45] Hence, the studies of in situ growth or phase transformations always involve high temperatures. For example, using curved graphitic structures (such as nanotubes and onions) as reaction cells to synthesize new structures at high temperatures has been realized inside the TEM.[6,7,46,47] Given their low threshold energy for displacement, carbon

www.MaterialsViews.com

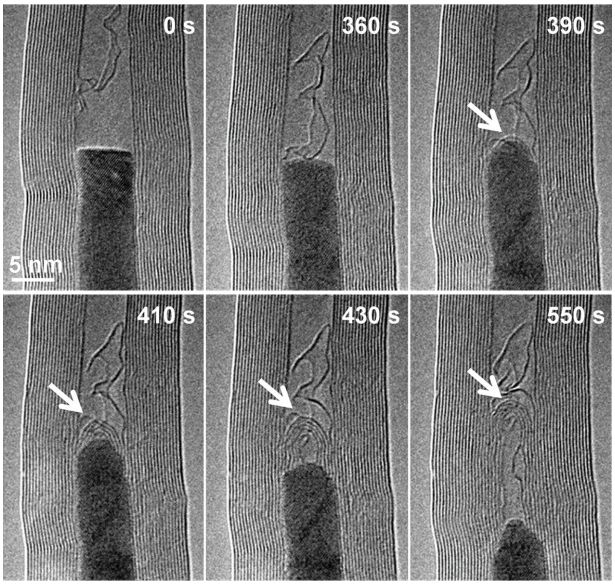

Figure 2. Growth of a multiwalled CNT from an FeCo crystal inside a large host nanotube under electron irradiation (50 A cm^{-2} to 120 A cm^{-2}) at a specimen temperature of 600 °C. The arrow points to the tip of the growing tube. Reproduced with permission.[7] Copyright 2007, Macmillan Publishing.

atoms are easily ejected into the core of C cages. When the cages are filled with other materials, C atoms will be sputtered into the encapsulated materials, thereby leading to reaction or intermixing of the components. Continuous loss of C atoms and surface reconstruction will cause the shrinkage of graphite shells. The self-contraction of outer shells causes an enormous inward pressure in the interior, particularly when the cages are filled with other materials.[34,48,49] Accordingly, C cages can act as a rigid, temperature-resistant container that provides a continuous C source and a high-pressure environment. Using this principle, the reaction from iron to iron carbide (Fe_3C) inside carbon onions has been observed in detail.[6] Another example of the growth of carbon nanotubes (CNTs) is shown in **Figure 2**.[7] Given that the solubility of C atoms in transition metals is low, and their diffusion is fast, C atoms ejected into the encapsulated metals will segregate at the uncovered surface as extended arrays of C networks after a short time. Therefore, Fe, cobalt, nickel, and Fe/Co alloy particles encapsulated in host CNTs have been used to monitor the nucleation and growth process of CNTs in real time and at high resolution.[7] These two experiments craftily utilized a tube or onion structure as a template, and used the ejected C atoms from the shells as the growth source, thereby providing a method to study the nucleation and growth of C-based materials at the nanoscale. However, such a method is limited to growing materials with the same components as the template.

The growth of 2D graphene,[50,51] silicon oxide,[52,53] and Fe[54] layers on substrates have been observed in TEM using the above mentioned principles. This method can be applied to the growth of 2D materials because we can introduce nearly all solid sources on planar substrates. Furthermore, substitution doping can also be observed inside the TEM when the vacancies generated by electron irradiation are filled with heterogeneous atoms.[55,56] For example, boron and nitrogen vacancies would be filled by C atoms—thereby eventually forming a BCN sheet—when a BN sheet loaded with paraffin wax as a C source was exposed to the electron beam.[56] Such electron irradiation-assisted doping indicates a pathway for the design and synthesis of in-plane heterostructures.

Most of the growth processes mentioned above are governed by elastic scattering processes. Inelastic scattering collisions can produce radiolysis effects, such as electrostatic charging, which can also stimulate the growth of some materials by electrostatic interactions.[8,11,57] The growth of magnesium oxide (MgO) on the surface of MgO crystals coated with platinum particles is undoubtedly supporting evidence.[8] As shown in **Figure 3**, capped MgO nanorods started growing from Pt particles, and kept growing with continuous irradiation. The nanorod formation and growth can be explained by electrostatic interaction mechanisms. Under electron irradiation, MgO particles are charged positively, whereas the Pt particles may possess negative charges because of the secondary electrons emitted by the trapped MgO particles. The positively charged MgO species can be attracted by the negatively charged metal particles, and trapped at the boundary between the particles. Consequently, the MgO builds a crystallographic lattice epitaxially underneath the metal particle.[8] Similarly, sodium nanostructures can grow on sodium chloride powder, driven by electron irradiation-induced charge and electrostatic effects.[11] These two experiments are driven by electrostatic interactions after

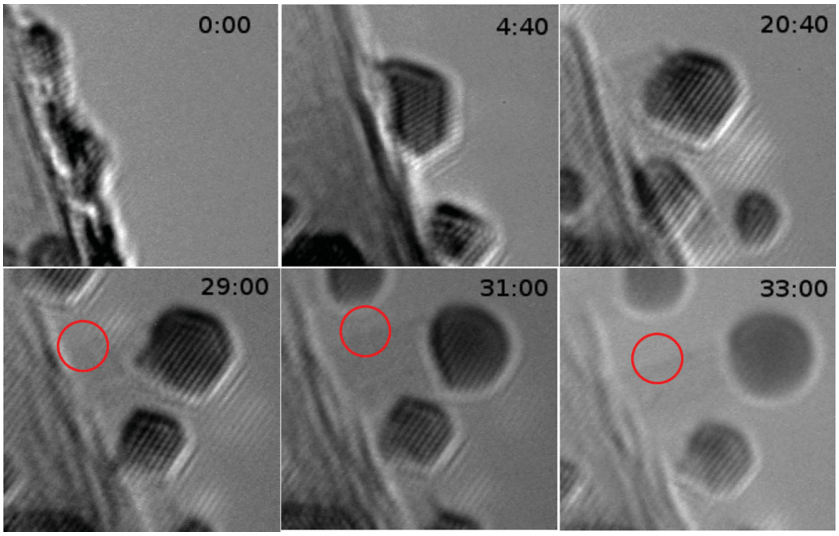

Figure 3. Growth of MgO nanorods on MgO substrate with Pt particles at room temperature. Beam current density: 200 A cm^{-2}. Each image represents an area of 9.2×9.2 nm^2. The red circles show the edges of the MgO nanorod. Reproduced with permission.[8] Copyright 2009, American Chemical Society.

the substrate is charged by the electron beam. The results of the above mentioned studies allow further investigations into the growth of nanorods with a small length–diameter ratio.

2.2. Gas Phase Growth

To introduce gas into the specimen area, while the other parts of the microscope column remain in high vacuum, two technologies have emerged over the years. One is the building of an environmental cell with an electron-transparent window, which is loaded at the tip area of the TEM holder. The specimen and gas are contained inside the cell without leaking into the column, due to the isolation effect of the window. This window-type environmental cell can provide a gas pressure of up to 1 atmosphere around the specimen.[26] Another approach is to modify the microscope pumping system, allowing for a gas pressure of up to 20 mbar in the specimen chamber.[26] These technical breakthroughs have promoted the investigation in structure evolution, nanocrystal growth, catalysis process, and oxidation/reduction behaviors.[14–19,58–69]

Generally, vapor phase growth can be carried out by exposing the heated sample to a reactive gas precursor inside the TEM. The precursor molecules are decomposed by the electron beam or thermal excitation, then the growth species is released, and deposited at a favorable location. For example, growth of 1D carbon nanostructures from decomposition of methane (CH_4) or acetylene (C_2H_2) on nanocatalysts has been performed to address the surface process.[14,70–72] Helveg et al. used a 1:1 mixture of CH_4/H_2 (at a total pressure of 2 mbar) as the reactive gas, and Ni as a catalyst, then monitored the formation of carbon structures on the Ni surfaces in real time.[14] In situ observations demonstrated that step edges act as a growth centre for graphene growth. Similarly, Sharma et al. also employed environmental TEM to evaluate the catalytic activity of Au, Ni, and Au-Ni nanoparticles for the formation of 1D carbon nanostructures from C_2H_2.[70] Both the real-time observations and density functional theory calculations revealed that small levels of Au doping in Ni increased the yield of 1D carbon nanostructures.[70] It is worth noting that the residual hydrocarbons in the microscope chamber, or on the surface of the substrate, can also be used as gaseous source to grow carbon nanostructures, although the growth kinetics is hard to quantitatively analyze.[73,74]

Another excellent example is the growth of silicon nanowires from disilane (Si_2H_6) using Au, Cu, and Pd catalysts.[16,75–83] Hofmann et al. observed the nucleation and growth of Si nanowires from Pd catalysts.[16] They found that the catalyst–Si interface free energies were lowest for atomically flat interfaces, and that the interfaces advanced via the lateral propagation of ledges.[16] On the basis of their experimental results, they proposed that growth by ledges was an important part of the vapor–solid–solid growth mechanism.[16] Some other in situ experiments have been performed inside the TEM to demonstrate vapor–liquid–solid growth. A sequence of distinct growth modes in Si nanowires were observed and proposed—such as angled and sawtooth modes[77] and jumping-catalyst modes,[79]—promoting the basic understanding of the physics of crystal growth.

2.3. Liquid Phase Growth

The gas cells can also be modified to accommodate liquids. So liquid phase crystal growth can be carried out in liquid cells, and monitored in real time inside the TEM.[20–24,84–92] The liquid cell based on silicon microfabrication technology was first designed by Williamson et al.[84] In their liquid cell design, two Si wafers coated with 100 nm Si_3N_4 were used as the main frame. Selective etching was adopted to form a viewing window on each wafer, and two reservoirs were etched on one wafer to supply liquid electrolyte. On the other wafer, a 0.5–1 μm SiO_2 ring spacer was patterned, forming a container between the two wafers after they were glued together. However, the spatial resolution was only 5 nm, depending on the thickness of the Si_3N_4 membranes and the liquid layer.[84] Using this method, Williamson et al. observed the nucleation and growth of nanoscale Cu clusters on a Au electrode during overpotential electrochemical deposition.[84] They found that the nucleation shared the characteristics of a homogeneous process, with many equivalent sites available, and that cluster growth was by equipartition of the available material flux over the cluster surface areas.[84]

Following the same concept, but reducing the thickness of the window membranes and spacers, the spatial resolution of liquid TEM characterization was improved to sub-nanometer by Zheng et al.[20] Using this improved-resolution liquid cell, they probed the growth kinetics of Pt nanocrystals. The in situ observation demonstrated that Pt nanocrystals could grow either by monomer attachment from solution, or by particle coalescence. With further improvement of the spatial resolution, the same method was then applied to study the real time growth of Pt_3Fe nanorods and Pt nanocubes at atomic resolution.[21,24] In particular, the observation of Pt nanocube facet development revealed that the conventional surface energy minimization law breaks down at the nanoscale.[24]

Graphene liquid cells are another feasible design for observation of crystal growth with atomic resolution. Because of its high shape flexibility, high mechanical tensile strength, and impermeability to small molecules, atomic layer graphene is considered to be a perfect support material for encapsulating a liquid solution. Additionally, electron scattering from the graphene membrane is negligible because of the atomic thickness, which ensures image quality and resolution. Graphene liquid cells were first designed and employed by Yuk et al.[22] to explore the mechanism of colloidal Pt nanocrystal growth.Some critical steps in nanocrystal coalescence were directly observed at the atomic level, including site-selective coalescence, structural reshaping after coalescence, and surface faceting.[22]

3. Nanofabrication with Atomic Resolution

As described above, irradiation effects occur in nearly all TEM systems. When the electron energy is higher than the threshold energy for atomic displacement, the atom will be knocked away from the lattice, thereby indicating the possibility of modifying specimens at the nanoscale. The capability of a modern TEM to focus the electron beam onto a spot that

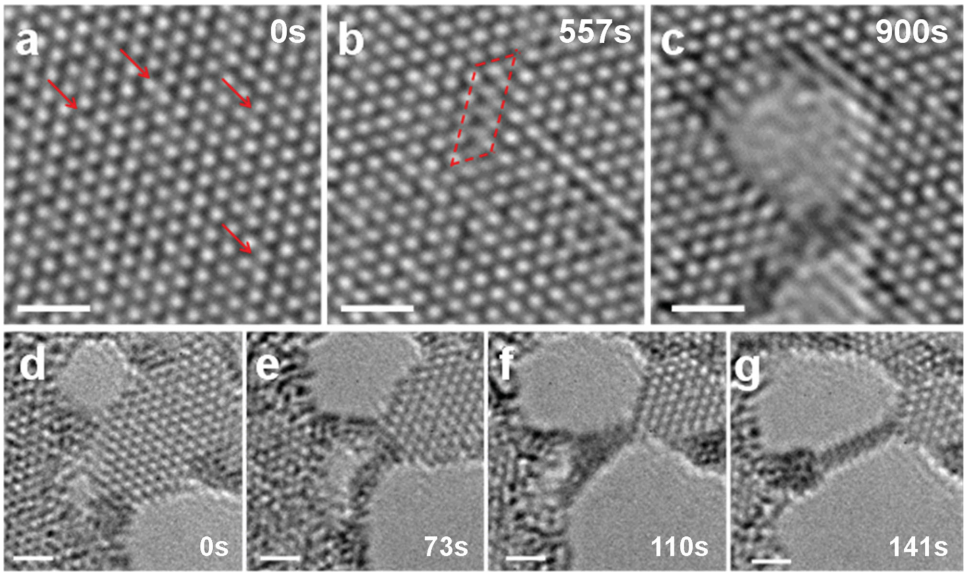

Figure 4. Structural evolution of MoS_2 monolayer under electron beam irradiation. a–c) S vacancies were aggregated and transformed to an extended line defect or nanopore under 80 kV electron irradiation (3 A cm^{-2}). Scale bar is 2 nm. Reproduced with permission.[97] Copyright 2013, Macmillan Publishing. d–g) As the nanopores expanded, the bridges between adjacent pores narrowed to nanoribbons. Beam current density: 40 A cm^{-2}. The ribbons showed high crystalline perfection. Scale bar is 2 nm. Reproduced with permission.[98] Copyright 2013, Macmillan Publishing.

is less than 1 Å in diameter suggests the possibility of using the beam to engineer materials at the atomic scale.[93–96]

Electron irradiation effects are heavily dependent on beam conditions. Therefore, the beam brightness, diameter, and electron energy should be adjusted to obtain a suitable range for different fabrications. For example, an electron beam with a moderate intensity has been widely used to study the formation of defects.[3,4,97] With continuous irradiation, the defects diffuse and agglomerate and subsequently form complex defects.[97–100] An experiment involving a monolayer of molybdenum disulfide (MoS_2) exposed to an electron beam is shown in **Figure 4**.[98] Sulfur vacancies (SVs), which can be distinguished by analysis of the intensity profile,[97,101] aggregated, transforming into an extended line defect and nanopore (Figure 4a–c). While the pores are growing, the bridges between adjacent pores narrowed to nanoribbons (Figure 4d–g). The ribbons showed high crystalline perfection that was different from MoS_2, and had higher stability than MoS_2 sheets when they were narrowed to sub-nanometer under electron irradiation.[98] Further in situ electrical measurements demonstrated that the ribbons were metallic, thereby providing a new building block for nanodevices.[102] Similarly, C atomic chains, C onions, and CNTs have been obtained from a few layers of graphene using a mild electron beam.[9,103–105] All these experiments show a novel top-down route for fabricating functional building blocks.

In another excellent example, CNTs were welded by a mild electron beam to form a molecular junction.[106,107] Perfect tubes would never join, but the vacancies introduced by the electron beam promoted the coalescence of the crossed nanotubes. The heterojunctions between CNTs and different metal nanocrystals could also be controllably formed via intense electron irradiation at the metal–nanotube contact areas.[108–110] Both metallic conductivity and covalent metal–C interfaces are essential for the application of such heterojunctions as contacts in electronic devices.

Irradiation with focused electron beams has also been used to tailor nanostructures. For example, CNTs can be bent when the beam is focused on one side of the tube,[111] and be cut when the focused beam is moved along the radial direction of the tubes.[112] Another excellent example is the nanopore, which can be sculpted in a variety of specimens inside the TEM, because the threshold energy for sputtering most existing elements is below 300 keV.[2,113–115] **Figure 5**

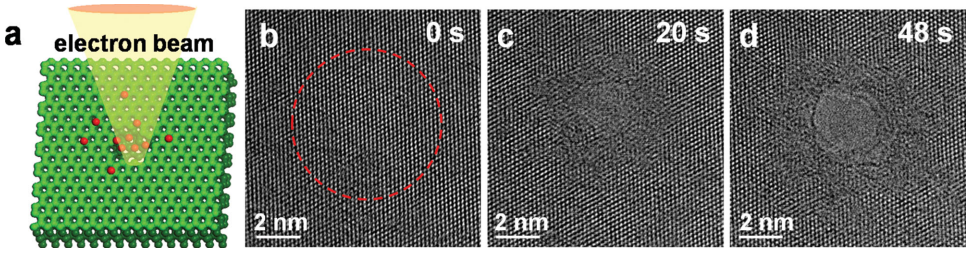

Figure 5. Fabrication of nanopores in the graphene sheet. a) Schematic diagram of the formation of nanopores on the graphene. b) Pristine graphene before high-dose electron irradiation. The dashed ring highlights the region to be irradiated. c,d) The same region as in (b) after electron irradiation, demonstrating that the irradiated area is damaged gradually, ultimately forming a nanopore. The beam current is about 2.0×10^3 A cm^{-2}. Reproduced with permission.[116]

demonstrates the formation of graphene nanopores by a focused electron beam. Figure 5b shows pristine graphene before electron irradiation. Then, the electron beam was focused within the area indicated, with a current density of 2.0×10^3 A cm^{-2}. The irradiated area was gradually damaged, and ultimately formed a nanopore.[116] However, the pore size—which is a significant parameter because of its potential application in selective translocation of molecules—is not fully controllable, because real-time imaging cannot be performed synchronously with drilling. Thermal excitation can be adopted to modulate the size of as-fabricated pores, as it promotes the migration and reconstruction of defects. Consequently, graphene nanopores could shrink or expand by direct thermal excitation, depending on the ratio of nanopore diameter to membrane thickness, thereby making the electron beam-based fabrication much more controllable.[117]

All fabrications described above make use of electron beam-induced displacement and sculpting, which remove unnecessary atoms. To obtain the desired morphology, mass loss and gain are both necessary to shape the features. Such a process can also be achieved inside the TEM, in which hydrocarbon molecules adsorbed on the specimen surface are polymerized and deposited by electrons. C tubular structure examples are shown in **Figure 6**.[74] The tubular structures were formed by electron beam-induced deposition on the surface of Te nanowires or nanotubes, with the subsequent removal of the core material by direct or Joule heating. Diverse tubular structures, such as co-axial hollow (Figure 6a), X-shape and Y-shape connected tubular (Figure 6c,d) could be formed by controlling the template shape.[74] Furthermore, the deposited amorphous C can be an excellent adhesive for joining or shaping features to a desired morphology.[118,119]

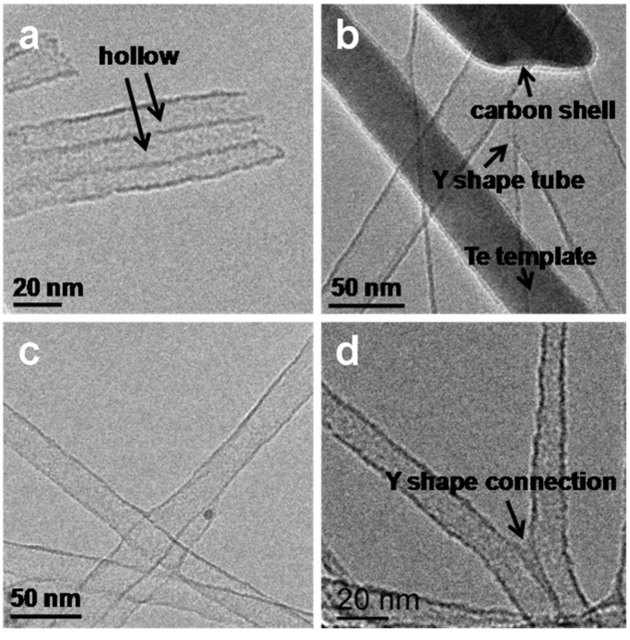

Figure 6. Fabrication of diverse tubular carbon structures using Te nanowires and nanotubes as templates. a) Fabricated co-axial hollow tubular structures with Te nanotube as template. b) Te-C core-shell wires. c,d) X-shape and Y-shape connected tubular structures. Reproduced with permission.[74] Copyright 2012, Elsevier.

Both displacement and deposition occur simultaneously inside the TEM, but they play leading roles in different circumstances.[116] Deposition is much more obvious than displacement when the beam current density is less than the critical value; otherwise, displacement is significant. Therefore, combining sculpting and deposition by adjusting beam brightness and diameter is an effective strategy for fabricating complex spatial structures.

4. In Situ Property Characterization

Characterization of nanostructure responses to stimuli from the surrounding environment at the nanometer scale will play a crucial role in further understanding the relationship between the structure and properties of nanomaterials. However, while conventional TEM has focused much on atomic structures, little focus has been placed on property measurements. To study the properties and behavior of individual nanostructures in external fields, a corresponding specimen holder should be designed depending on the external load. Most of the in situ TEM technologies are based on the elegant design of specimen holders, such as those used for in situ heating, biasing, and mechanical TEM.[26]

4.1. Thermal Property Characterization

Nowadays, materials' response to thermal excitation can be investigated in situ on the nanoscale inside the TEM by using heating and cooling stages. Generally, heating can be done by placing a heating element at the tip of TEM specimen holder. A popular design the use of a heating-filament-embracing specimen disk as an electric furnace and embedded thermocouple, in order to measure the temperature in the furnace cup. This type of heating stage is commercially available and allows heating of the specimen up to 1300 °C, which is sufficiently high for studying thermal properties (such as thermal stability) of materials as well as thermal excitation-induced behavior.[120–125] For example, Au nanorods could change their shape at a temperature of approximately 380 °C, which was much lower than the bulk melting point of Au (1063 °C); however, thermal stability could be enhanced by a thin amorphous C shell coating on the on Au surface.[121] In another excellent example, the thermal excitation-induced phase transition of VO_2 was monitored,[120] as shown in **Figure 7**. Both the TEM image obtained at room temperature (25 °C) and the corresponding fast Fourier transform (FFT) pattern revealed that the VO_2 specimen is initallay in the monoclinic (Figure 7a). As the temperature increased to 50 °C, the monoclinic VO_2 phase gradually decreased while the rutile phase emerged (Figure 7b). The coexistence of the monoclinic and rutile phases in the same TEM image demonstrated that the phase transition of VO_2 from the monoclinic phase to the rutile phase was already underway at 50 °C. When the temperature was raised to 70 °C, only the rutile phase could be observed, which demonstrated that the phase transition

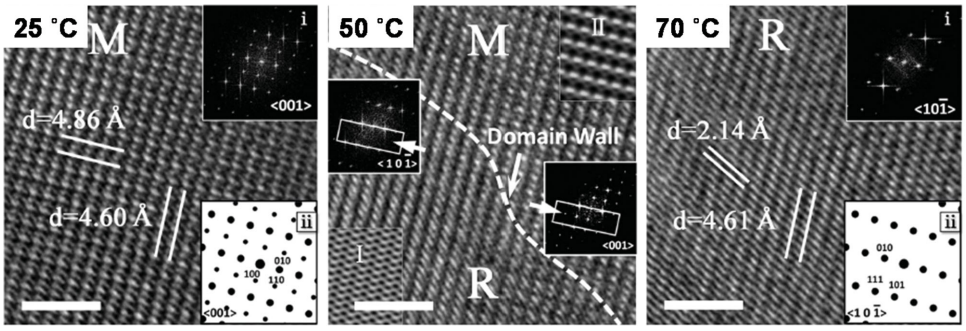

Figure 7. TEM images of VO_2 at different temperatures, showing the phase transition during the heating process. a) TEM image of monoclinic VO_2 at 25 °C. The insets show the corresponding i) FFT image and ii) simulated electron diffraction patterns. b) TEM image at 50 °C demonstrating that the phase transition has occured at 50 °C. The domain wall is indicated by a dotted line. Insets show corresponding FFT and simulated TEM images of (I) rutile and (II) monoclinic phases. c) TEM image of monoclinic VO_2 at 70 °C. The insets show the corresponding i) FFT image and ii) simulated electron diffraction patterns. Scale bars are 2 nm. Reproduced with permission.[120] Copyright 2014, Macmillan Publishing.

had been completed. Combining this with ab initio simulations, He et al. proposed that the transition process included movement of V–V pairs and expansion along the *c*-axis of the monoclinic phase.[120]

A particular problem exists in high-temperature microscopy. The drift of the image, introduced by thermal expansion of the stage and the specimen material itself, can be serious in high-resolution microscopy. Water cooling of the specimen holder rod is usually applied to maintain the low temperature of the body, but this device causes mechanical vibrations in the system.[4] An alternative approach is to study the thermal properties directly using the Joule heating of nanomaterials when a bias voltage is applied. To generate Joule heat, a closed circuit should first be set up. A probe TEM specimen holder is generally a good choice for this purpose. A built-in metallic probe with a tip can be moved back and forth in fine steps controlled by a piezo manipulator. Thus, contact is possible between the probe and the nanostructure. The probe is connected to a power supply unit by which a voltage can be applied to the specimen. However, the Joule heating induced local temperature rise within the specimen cannot read directly;a reference temperature field should be set up around the specimen. Generally, Au or Pt particles deposited on the specimen surface are adopted, such that Joule heating induced evaporation of these particles is used to reflect local instantaneous temperature.[126,127] Joule heating-induced local temperatures can be increased to higher than 1500 °C with small specimen drift, thereby indicating that this method is a good choice for conducting in situ thermal experiments. For example, when a constant bias of 2.3 V is applied on a single-walled CNT with 12 nm diameter and 24 nm length, the Joule heating-induced temperature increase is approximately 2000 °C inside the nanotube.[128] The CNT can be unzipped under such a high temperature.[129] Some other phenomena induced by Joule heating have been observed inside the machine, such as the sublimation of suspended few-layer graphene.[126,130] Huang et al. found that the graphene sublimation fronts consisted of mostly zigzag edges, and that more than 99% of the graphene edges observed during sublimation were bilayer edges rather than monolayer edges.[130]

4.2. Electrical Testing

If the thermal measurement probe holder described above in Section 4.1 is connected not only to a power supply unit but also to an electrical measuring unit, the electrical response of the materials and corresponding electrical parameters can be observed and measured directly inside the TEM. Such a probe system has been widely used to study the behavior and structural changes of specimens in an electrical field, as well as the electrical transport properties of individual nanostructures. For example, when a bias voltage is applied to a nanostructure synthesized inside TEM, the electrical conductivity can be obtained directly.[102,131] Therefore, both synthesis and property characterization can be realized inside the same equipment, which is important for guiding the design of materials with novel properties, and nanodevices based on a single nanostructure. This probe system has also been widely used to study the behavior of nanodevices, and their failure mechanisms, for applications such as memory, nanobatteries, and so on. More detailed examples will be given in Section 5.

Another noteworthy phenomenon under application of a bias voltage is mass transportation.[132–140] Electromigration—one of the most popular mechanism to explain the mass transportation—is a process of directional material flow induced by an electric current; this process is observable only at elevated temperatures and at high current densities.[141] Regan et al. were the first to report controllable and reversible atomic scale mass transport along the CNTs inside the TEM, using indium metal as the prototype transport species.[132] Although the exact nature of the driving mechanism was not very clear, Regan et al. considered that electromigration model was perhaps more analogous to the in situ experiments.[132] Soon afterwards, Svensson et al. demonstrated experimentally that CNTs can be used as "nanopipettes", in order to deposit and retrieve solid material on a nanometer scale inside the TEM.[133] The process relied on the electromigration force, which is created at high electron current densities, enabling the transport of materials inside the hollow core of CNTs.[133] Further in situ experiments found that the metal nanocrystal remained largely solid and crystalline when the crystal was bodily transported inside the

CNTs.[138,139] Motion and rearrangement of metal atoms on the crystal surface were considered to be the main reason for this. However, Zhao et al. found that not only electromigration but also thermomigration or thermal evaporation caused by Joule heating could induce mass transportation.[142] Zhao et al. further discussed the competitive relationship between the thermal gradient force and electromigration, force and concluded that the thermal gradient force overrides the electromigration force in most conditions.[142]

4.3. Mechanical Testing

Mechanical properties may change significantly when the size of a material is reduced to the nanoscale, because many fundamental assumptions of classical mechanics fail. To investigate the mechanical behavior and corresponding structural changes in nanostructures, a dedicated mechanical holder should first be designed. The key to a mechanical holder is the loading of a tensile or compressive mechanical force on the specimen, while tracking the structural changes in real time.

The probe holder is one of the most popular designs because additional mechanical force can be introduced by back and forth movement of the probe, and has been widely used to study mechanical behaviors, such as deformation, inside the TEM.[143–148] Using a probe holder, Wan et al. found that Na nanostructures grown from NaCl powder revealed superplastic elongations of 300% under the influence of tension.[11] Zheng et al. utilized the same holder to reveal deformation processes in nanometer-sized Au crystals.[146] They found that partial dislocations located at the free surfaces dominated the plastic deformation of Au nanocrystals.[146] Further in situ experiments revealed the nucleation, migration and annihilation of the dislocation-originated stacking fault in tetrahedral Au nanocrystals, uncovering a unique deformation mechanism via dislocation interactions inside the confined volume of nanocrystals.[143] Another noteworthy phenomenon is liquid-like pseudoelasticity, which was first observed by Sun et al. when an external mechanical force was applied to a sub-10 nm crystalline Ag particle,[147] as shown in **Figure 8**. From the cycle of compression (Figure 8a–e) and stretching (Figure 8f–i) of the Ag crystal, Sun et al. found that Ag nanoparticles could be deformed like a liquid droplet, but these nanoparticles retained their highly crystalline form in the interior, with no sign of dislocation activity during deformation.[147] Combining these observations with atomistic simulations, Sun et al. concluded that the shape change of such small particles was dominated by surface diffusion.[147]

Recently, another innovative in situ mechanical testing method based on the TEM grid has been developed by Han et al.[149–154] Nanowires are scattered randomly on the TEM grid, then covered with a colloidal thin film, which could curl or shrink under electron irradiation or thermal excitation. As a result, some wires are wrapped in the curled thin films, thereby being bent or subjected to an axial tensile force. Using this method, in situ tensile and bending experiments have been performed on Si nanowires, silicon carbide (SiC) nanowires and Ni nanowires.[149–154] They found that the continuous plasticity of Si and SiC nanowires was accompanied by a process of increased dislocation density in the early stages, followed by an obvious lattice distortion, finally reaching an entire structure amorphization in the most strained regions of the nanowires.[151,152] They also found that partial and full dislocation nucleation, motion, escape, and interactions were responsible for the ultra large strain—up to 14% in bent Si nanowires.[154]

The methods mentioned above have an obvious deficiency, which is the inability to quantify the force load. To overcome this problem, a mechanical quantity sensor is integrated into the tip of the holder. By using this method, in situ tensile tests have been performed on CNTs,[155] BN nanotubes,[156] WS_2 nanotubes,[157] and other 1D or 2D nanostructures.[158–162] In situ nanoindentation tests can also be performed inside the TEM using a similar holder.[163–167] Shan et al. applied a compression force to a nanocrystalline cadmium sulphide (CdS) hollow sphere and recorded the dynamical process.[163] They found that the CdS hollowed sphere was capable of withstanding extreme stress (approaching the ideal shear strength of CdS).[163] Using the same method, a series of in situ nanoindentation experiments were performed on pillar metal samples.[164–167] Many interesting phenomena, such as mechanical annealing in both face centered cubic and body centered cubic metals,[164,167] stress saturation, and deformation mechanism transitions were observed.[165]

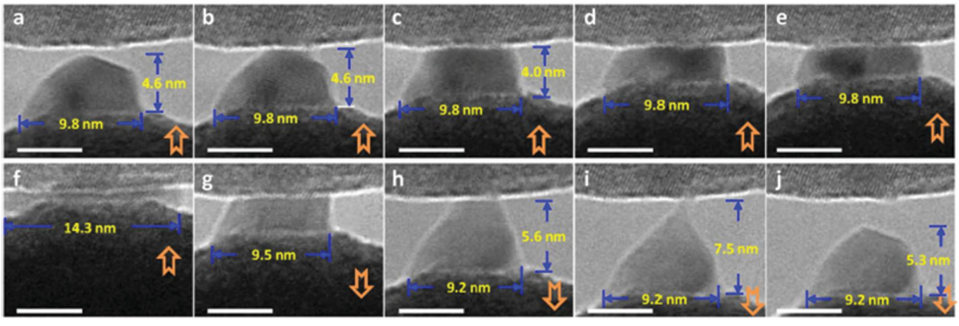

Figure 8. Reversible pseudoelastic deformation of a Ag nanocrystal. a) Initial geometry of the Ag nanocrystal. The diameter of the base is 9.8 nm and the height is 4.6 nm. b–i) Dynamic shape evolution of the Ag nanocrystal during compression and stretching. The base part retains its size in the first stages of compression, and later turns to a pancake-like structure. During stretching, the base almost recovers its initial size, with a slight decrease in diameter, from 9.8 to 9.2 nm. j) Final geometry of the Ag nanocrystal. All scale bars are 5 nm. Reproduced with permission.[147] Copyright 2014, Macmillan Publishing.

Additionally, many other designs for in situ nanomechanical TEM holders have been proposed.[26,27,168] Using these dedicated holders, many in situ mechanical tests have been conducted inside the TEM. Considerable experimental details can be found in previous specialized reviews or book chapters.[169–172]

4.4. Testing Other Properties

Light can also be introduced into the specimen chamber via optical fibers, or by adding an LED on the tip of the holder, thereby allowing the study of light-induced phenomena in photoactive materials and photocatalysts under their working conditions.[173–175] External magnetic fields can be applied to the specimen by the addition of Helmholtz coils on either side of the specimen, or by bringing the piezo-driven sharp needle (comprising a permanent magnet) close to the specimen, thus, studying the magnetization dynamics and some other magnetic phenomena at the nanoscale becomes possible.[26,176,177]

5. Nanodevice Construction

A thorough knowledge of the structure–property relationship is insufficient in nanomaterial research. The ultimate goal is the efficient use of materials and natural resources. Towards this goal, and to further understand the relationship between property and function, nanodevices are set up inside the TEM to study their functions and working/failure mechanisms. Based on the material properties, TEM holder design, and method of preparation of specimens, many nanodevices may be set up inside the TEM. In this section, we focus on three types of device: nanoextruders, random access memory, and nanobatteries.

5.1. Nanoextrusion

As described in the growth section, intense electron irradiation would cause shrinkage of a CNT or C onion. The self-contraction of the outer shells causes an enormous inward pressure in the interior at high temperatures, particularly when the cages were filled with C or other materials.[6,34,48,49] Based on these experiments, C cages can be used as nanoextruders to study the mechanical behavior of the encapsulated materials.

Figure 9 shows that when a CNT is partly filled with a Fe_3C nanowire and placed under electron irradiation at 600 °C, the collapse of the tubes leads to a pressure of 20–40 GPa, which pinches and cuts off the encapsulated Fe_3C crystal (Figure 9a–d).[34] Similarly, self-compression of C onions has been used in several extrusion experiments when metal crystals are encapsulated inside the graphitic shells.[48,178] As reported by Sun et al.,[48] the particles (including Au, Pt, Mo, and W) encapsulated inside graphitic shells became spherical under electron irradiation in a wide beam, due to the surface stress exerted by the graphitic shells during removal of atoms and reconstruction. A hole was drilled into one side of the onion, using a focused electron beam with a diameter of 2 nm. The material under pressure could escape through the hole. During the continuing collapse of the shells, pressure build-up occurred, and the solid metal was gradually extruded through the hole. Due to the contraction of the graphitic shell, deformation occurred at a scale of 0.1 m s^{-1} to 1 nm s^{-1}, thereby allowing the detailed study of nanocrystal stability under continuous load conditions.

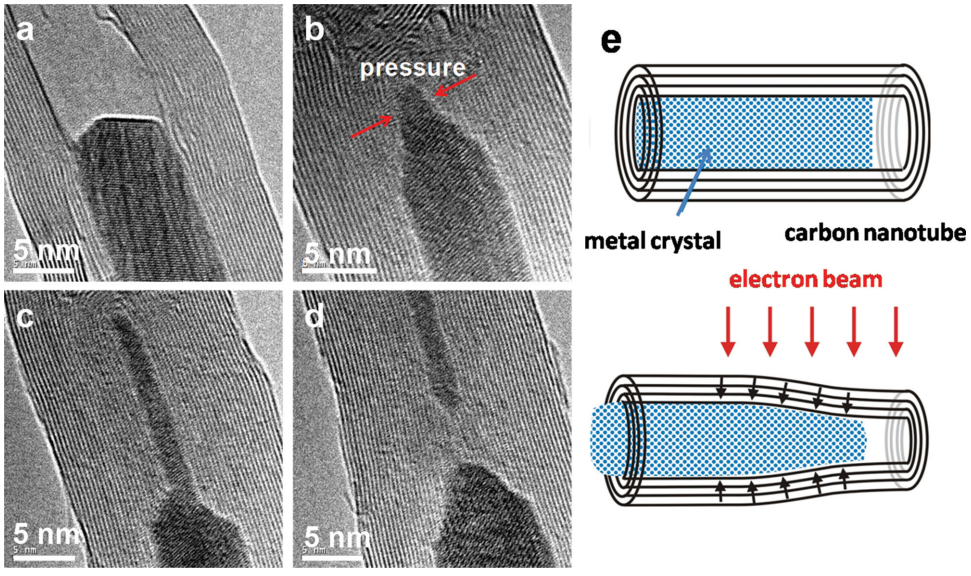

Figure 9. Electron irradiation-induced collapse of a carbon nanotube tube, and deformation of the encapsulated Fe_3C crystal. a) Tube before irradiation. b,c) Irradiation leads to the collapse of the tube, and deformation of the Fe_3C crystal. d) Tube collapse cuts off the thinned Fe_3C crystal. e) Schematic diagram indicates how contraction of the tube deforms and extrudes the encapsulated Fe_3C crystal. Reproduced with permission.[34] Copyright 2006, American Association for the Advancement of Science.

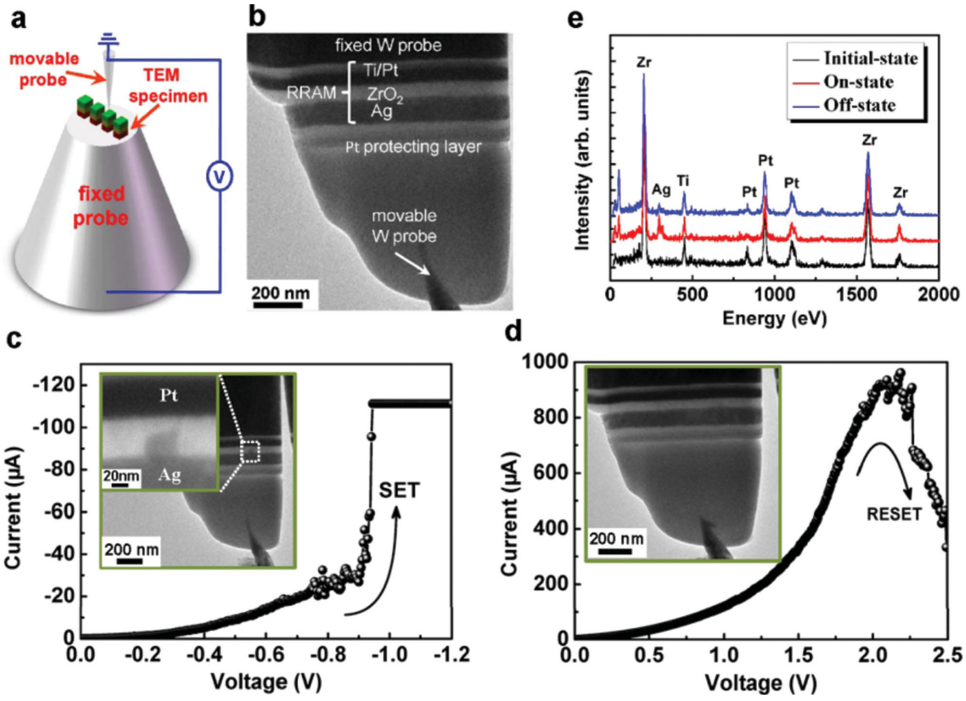

Figure 10. Resistive switching behavior and corresponding structural changes during in situ electrical tests. a) Schematic of the in situ TEM experimental set-up. b) Cross-sectional image corresponding to a fresh Ag/ZrO_2/Pt memory device. c) Current–voltage (*I–V*) curve of the memory device during SET operation. The inset shows the TEM image of the device after the SET process. d) *I–V* curve of the device during a RESET operation. The inset shows the TEM image after the RESET process. e) EDX analysis of the device conducted at the initial-, ON- and OFF-states. The EDX spectra were sequentially obtained at the conductive filaments region with a 30 s acquisition time, using a 20 nm electron beam. Reproduced with permission.[37]

5.2. Random Access Memory

Modification of the TEM holder and methods of preparation of the specimen allow the establishment and functionality of more devices inside the machine. For example, using a probe holder, a specially-developed resistive memory was used to study the switching characteristics and physical mechanism.[37,179–185] As shown in **Figure 10**, Liu et al. demonstrated an oxide-electrolyte-based resistance random access memory (ReRAM), fabricated directly onto the W probe (Figure 10a,b), applying a bias voltage to the Ag/ZrO_2/Pt memory.[37] When the magnitude of the negatively biased voltage exceeded the threshold voltage, as shown in Figure 10c, conductive filaments formed inside the solid-electrolyte layer and connected the two electrodes, thereby indicating that the device switched from the high-resistance (OFF) state to the low-resistance (ON) state. When a positive voltage was applied (Figure 10d), the device switched back to the OFF state because of the dissolution of the conductive filaments. The energy dispersive X-ray (EDX) spectra obtained from the conductive filaments region in the initial-, ON- and OFF-states shows that no Ag signal was found in the initial-state in the ZrO_2 film, but a Ag signal was present in the ON-state. However, the Ag atoms in the conductive filaments cannot be re-collected into the Ag electrode because of the weak Ag signal in the OFF-state. The density of residual Ag atoms would increase with the number of switching cycles.[37] Liu et al. proposed a modified microscopic mechanism based on the local redox reaction inside the ZrO_2-electrolyte system to account for observed resistive switching effect.[37] Such a method contributes to a comprehensive understanding of resistive switching behavior, which will serve as a guide for enhancing performance and reliability of ReRAM and for further promoting the rapid development of a universal non-volatile memory system. Using the same principle, a kind of memristive abacus device, based on synaptic Ag–Ge–Se electrolytes, was observed inside the TEM.[186] The conductive Ag_2Se dendrite formed and dissolved when positive and negative biases were applied on the Ag electrode. The bias-driven phase transformation caused memristive long-term potentiation and depression.

5.3. Nanobatteries

With the development of in situ techniques, nanobatteries can be set up inside the TEM, allowing for real-time and atomic-scale observations of battery charging and discharging processes.[187,188] It provides not only a deeper understanding of the fundamental sciences of batteries, but also critical guidance in development of advanced batteries. Two types of nanobattery cells based on different types of electrolyte have been created inside the TEM, one based on liquid (including room temperature ionic liquid) electrolytes,[36,38,189–197] and the other based on all solid components.[197–217]

Designing and setting up liquid-electrolyte-based devices inside TEM is necessary to investigate the behavior of electrochemical devices at the nanometer scale. However, liquid

is generally difficult to preserve in vacuum because of high vapor pressure, as described in the growth section. Making the liquid electrolyte work in the machine is the principal challenge. One method for solving this problem is to use room-temperature ionic liquids. Given ultralow vapor pressure, ionic liquids can be handled in a vacuum. Huang et al. set up a nanoscale-electrochemical device (consisting of SnO_2 nanowire as an anode, ionic liquid as electrolyte, and a $LiCoO_2$ particle as a cathode) inside the TEM to enable direct real-time visualization of the structural changes during electrochemical charging.[36] Huang et al. found that the reaction front is a "medusa zone", containing a high density of mobile dislocations. The dislocation cloud functioned as a structural precursor to an electrochemically driven solid-state amorphization, which is the major effect that plagues the performance and lifetime of anodes in Li-ion batteries.[36] Further experiments found that the Li_xSn phase possessed a spherical morphology, and was embedded into the amorphous Li_yO matrix.[191] The charging rate could also be dramatically altered by coating the SnO_2 nanowires with carbon, aluminum, or copper.[192] Following the same concept, but changing the anodes materials, Liu et al. observed the electrochemical lithiation of individual Si nanowire anodes.[190] They found that carbon coating and phosphorus doping resulted in a order of magnitude increase in the charging rate.[190] These experiments provide important mechanistic insights towards the design of advanced batteries.

As an alternative approach, application of the electrochemical liquid cell is a much more universal technique for liquid-based devices, as the liquid can be sealed in a Si-based cell and isolated from the vacuum. Using this principle, a Li-ion battery with a commercial liquid electrolyte was set up inside the machine.[38,195,196] These experiments elucidated several strategies for improving the performance of commercial Li-ion batteries.

Solid battery cell experiments are another important group of experiments that can be conducted inside the TEM, and are applicable to both Li-ion batteries[197–211] and Na-ion batteries.[213–217] Generally, in the Li-ion battery cell, Li metal is used as the reference electrode and lithium source, and the native Li_2O layer formed on the metal surface acts as a solid electrolyte. Using a Si nanowire as anode, Liu et al. studied the dynamic lithiation process with atomic resolution. They found that the migration of sharp interface (≈1 nm thickness, between the crystalline Si and the amorphous Li_xSi alloy) played an important role in the lithiation process.[202] The measurement of the growth rate of the amorphous Li_xSi layer during the first lithiation showed the self-limiting lithiation, which was attributed to the retardation effect of the lithiation induced stress.[201] They also observed anisotropic swelling of Si nanowires with intermediate dumbbell-shaped cross sections. The large tensile stress developed inside the nanowire may cause a necking instability and fracture.[197] Soon after, the experiments were extended to other anode materials systems, including germanium nanowires and nanoparticles,[198,207] gallium nanorods,[206] CNTs,[200] and aluminum nanowires.[199]

Following the same concept, but changing the reference electrode and electrolytes, Na-ion batteries have also been set up inside the TEM.[213–217] In these cells, Na metal is used as the reference electrode and sodium source, and the layer of sodium oxide (Na_2O) and hydroxide (NaOH) grown naturally on the metal surface acts as a solid electrolyte. Using tin nanoparticles as anode materials, Wang et al. studied the structural changes and phase transformations of Sn particles during electrochemical sodiation.[213] The first sodiation process occurred in two steps with a uncracked volumetric expansion of 420%; reversible sodiation/desodiation processes were demonstrated for Sn particles without fracture.[213] Soon afterwards, Han et al. found that Al_2O_3 coated Sn particles had remarkably high initial capacity and high capacity retention, compared with those made of bare Sn nanoparticles, which could be used to improve battery cycle performance.[215] Besides, the anode was replaced by some other materials, such as SnO_2,[214] FeF_2,[216] carbon nanofibers,[217] and performed inside the TEM.

6. Summary and Outlook

TEM is currently one of the most powerful analytical tools for structural characterization of nanomaterials with atomic-scale resolution. The development specialized specimen holder designs enables the application of external fields to specimens inside the TEM, thereby extending the capabilities of the TEM beyond static structural characterization to in situ observation of materials in stimulating environments. The atomic-scale visualization of the structural evolution of the specimen under operational conditions introduces new possibilities in the investigation of relationships among structure, unique properties, and functionality; essential in designing new materials and devices for the efficient use of our natural resources and a sustainable future.

Now, aberration corrected TEM and scanning TEM (STEM) equipped with high-resolution electron energy loss spectroscopy (EELS) enables the investigation of not only the structure, but also the elemental composition and chemical bonding of nanomaterials at the atomic scale. However, transient nucleation events during chemical reactions are still a great challenge to characterize in situ. Ultrafast TEM has achieved imaging with a spatial and temporal resolution of 10 nm and 10 ps respectively, representing a thousand-fold improvement over current TEM, which shows great potential in understanding the molecular dynamics of chemical reactions, in space-time mapping of lattice vibrations, and in recording so-called "hidden states" far away from equilibrium.[218] However, ultrafast TEM is still in its infancy, methods of imaging with atomic spatial resolution and ultrafast temporal resolution is a direction for further development in the future.

Another direction for furthering in situ TEM is the development of versatile sample stage and holder geometries, which will allow for the multi-modal probing of material functionality both in situ and in operando. The electron optics should encompass a pole piece that can accommodate the new stage, differential pumping, detectors, aberration correctors, and other electron optical elements for measurement of materials dynamics.[218] The combination of advanced

specimen holder design and instrument modification, means that more and more experiments will be possible inside the TEM, leading us to believe that all current experiments related to nanomaterials may be realized inside TEM in the near future; such that TEM may become a basic common tool utilized in the same way as normal optical microscopes are used in the lab now. Dynamic in situ experimentation on nanomaterials and the related instrumentation and techniques will undergo a rapid development and may be applied to a wide range of scientific research areas in future.

Acknowledgements

This work was supported by the National Basic Research Program of China (Grant No. 2011CB707601), the National Natural Science Foundation of China (Nos. 61274114, 113279028 and 51071044), the Natural Science Foundation and Qing Lan Project of Jiangsu Province (Nos. BK2011592, BK2012024), and the Scientific Research Foundation of Graduate School of Southeast University (No. YBJJ1329).

[1] F. Banhart, *Rep. Prog. Phys.* **1999**, *62*, 1181.
[2] R. F. Egerton, P. Li, M. Malac, *Micron* **2004**, *35*, 399.
[3] A. V. Krasheninnikov, K. Nordlund, *J. Appl. Phys.* **2010**, *107*, 071301.
[4] F. Banhart, in *In-Situ Electron Microscopy*, (Eds: G. Dehm, J. M. Howe, J. Zweck), Wiley-VCH, Weinheim, Germany **2012**, Ch. 5.
[5] A. V. Krasheninnikov, F. Banhart, *Nat. Mater.* **2007**, *6*, 723.
[6] L. Sun, F. Banhart, *Appl. Phys. Lett.* **2006**, *88*, 193121.
[7] J. A. Rodríguez-Manzo, M. Terrones, H. Terrones, H. W. Kroto, L. Sun, F. Banhart, *Nat. Nanotechnol.* **2007**, *2*, 307.
[8] A. G. Nasibulin, L. Sun, S. Hämäläinen, S. D. Shandakov, F. Banhart, E. I. Kauppinen, *Cryst. Growth Des.* **2009**, *10*, 414.
[9] A. Chuvilin, U. Kaiser, E. Bichoutskaia, N. A. Besley, A. N. Khlobystov, *Nat. Chem.* **2010**, *2*, 450.
[10] F. Börrnert, S. M. Avdoshenko, A. Bachmatiuk, I. Ibrahim, B. Büchner, G. Cuniberti, M. H. Rümmeli, *Adv. Mater.* **2012**, *24*, 5630.
[11] N. Wan, L.-T. Sun, X.-H. Hu, Y.-Y. Zhu, L. Zha, T. Xu, H.-C. Bi, J. Sun, F.-Z. Dong, *Cryst. Growth Des.* **2012**, *12*, 3899.
[12] K. Yin, Y. Xia, Z. Liu, J. Yin, L. Sun, *Phys. Status Solidi A* **2012**, *209*, 135.
[13] H. Zheng, J. B. Rivest, T. A. Miller, B. Sadtler, A. Lindenberg, M. F. Toney, L.-W. Wang, C. Kisielowski, A. P. Alivisatos, *Science* **2011**, *333*, 206.
[14] S. Helveg, C. Lopez-Cartes, J. Sehested, P. L. Hansen, B. S. Clausen, J. R. Rostrup-Nielsen, F. Abild-Pedersen, J. K. Nørskov, *Nature* **2004**, *427*, 426.
[15] S. Kodambaka, J. Tersoff, M. C. Reuter, F. M. Ross, *Science* **2007**, *316*, 729.
[16] S. Hofmann, R. Sharma, C. T. Wirth, F. Cervantes-Sodi, C. Ducati, T. Kasama, R. E. Dunin-Borkowski, J. Drucker, P. Bennett, J. Robertson, *Nat. Mater.* **2008**, *7*, 372.
[17] C. Kallesøe, C.-Y. Wen, K. Mølhave, P. Bøggild, F. M. Ross, *Small* **2010**, *6*, 2058.
[18] S. H. Oh, M. F. Chisholm, Y. Kauffmann, W. D. Kaplan, W. Luo, M. Rühle, C. Scheu, *Science* **2010**, *330*, 489.
[19] Y.-C. Chou, K. Hillerich, J. Tersoff, M. C. Reuter, K. A. Dick, F. M. Ross, *Science* **2014**, *343*, 281.
[20] H. Zheng, R. K. Smith, Y.-w. Jun, C. Kisielowski, U. Dahmen, A. P. Alivisatos, *Science* **2009**, *324*, 1309.
[21] H.-G. Liao, L. Cui, S. Whitelam, H. Zheng, *Science* **2012**, *336*, 1011.
[22] J. M. Yuk, J. Park, P. Ercius, K. Kim, D. J. Hellebusch, M. F. Crommie, J. Y. Lee, A. Zettl, A. P. Alivisatos, *Science* **2012**, *336*, 61.
[23] H.-G. Liao, H. Zheng, *J. Am. Chem. Soc.* **2013**, *135*, 5038.
[24] H.-G. Liao, D. Zherebetskyy, H. Xin, C. Czarnik, P. Ercius, H. Elmlund, M. Pan, L.-W. Wang, H. Zheng, *Science* **2014**, *345*, 916.
[25] A. Masseboeuf, in *Transmission Electron Microscopy in Micro-Nanoelectronics*, Wiley-ISTE, Hoboken, USA **2013**, Ch. 8.
[26] A. Ziegler, H. Graafsma, X. F. Zhang, J. W. M. Frenken, *In-situ Materials Characterization: Across Spatial and Temporal Scales*, Springer, Dordrecht, Netherlands **2014**.
[27] M. Haque, H. Espinosa, H. Lee, *MRS Bull.* **2010**, *35*, 375.
[28] B. Westenfelder, J. C. Meyer, J. Biskupek, S. Kurasch, F. Scholz, C. E. Krill, U. Kaiser, *Nano Lett.* **2011**, *11*, 5123.
[29] B. Barwick, H. S. Park, O.-H. Kwon, J. S. Baskin, A. H. Zewail, *Science* **2008**, *322*, 1227.
[30] F. Carbone, O.-H. Kwon, A. H. Zewail, *Science* **2009**, *325*, 181.
[31] A. H. Zewail, *Science* **2010**, *328*, 187.
[32] R. M. van der Veen, O.-H. Kwon, A. Tissot, A. Hauser, A. H. Zewail, *Nat. Chem.* **2013**, *5*, 395.
[33] U. J. Lorenz, A. H. Zewail, *Science* **2014**, *344*, 1496.
[34] L. Sun, F. Banhart, A. Krasheninnikov, J. Rodriguez-Manzo, M. Terrones, P. Ajayan, *Science* **2006**, *312*, 1199.
[35] C. T. Nelson, P. Gao, J. R. Jokisaari, C. Heikes, C. Adamo, A. Melville, S.-H. Baek, C. M. Folkman, B. Winchester, Y. Gu, Y. Liu, K. Zhang, E. Wang, J. Li, L.-Q. Chen, C.-B. Eom, D. G. Schlom, X. Pan, *Science* **2011**, *334*, 968.
[36] J. Y. Huang, L. Zhong, C. M. Wang, J. P. Sullivan, W. Xu, L. Q. Zhang, S. X. Mao, N. S. Hudak, X. H. Liu, A. Subramanian, *Science* **2010**, *330*, 1515.
[37] Q. Liu, J. Sun, H. Lv, S. Long, K. Yin, N. Wan, Y. Li, L. Sun, M. Liu, *Adv. Mater.* **2012**, *24*, 1844.
[38] Z. Zeng, W.-I. Liang, H.-G. Liao, H. L. Xin, Y.-H. Chu, H. Zheng, *Nano Lett.* **2014**, *14*, 1745.
[39] K. Min Jun, M. Ben, M. Kazuyoshi, M. Amit, *Nanotechnology* **2007**, *18*, 205302.
[40] A. J. Storm, J. H. Chen, X. S. Ling, H. W. Zandbergen, C. Dekker, *Nat. Mater.* **2003**, *2*, 537.
[41] H. Zheng, Y. Liu, F. Cao, S. Wu, S. Jia, A. Cao, D. Zhao, J. Wang, *Sci. Rep.* **2013**, *3*, 1920.
[42] S. Wu, F. Cao, H. Zheng, H. Sheng, C. Liu, Y. Liu, D. Zhao, J. Wang, *Appl. Phys. Lett.* **2013**, *103*, 243101.
[43] R. F. Egerton, *Microsc. Microanal.* **2013**, *19*, 479.
[44] Y.-C. Lin, D. O. Dumcenco, Y.-S. Huang, K. Suenaga, *Nat. Nanotechnol.* **2014**, *9*, 391.
[45] R. Boston, Z. Schnepp, Y. Nemoto, Y. Sakka, S. R. Hall, *Science* **2014**, *344*, 623.
[46] M. Koshino, Y. Niimi, E. Nakamura, H. Kataura, T. Okazaki, K. Suenaga, S. Iijima, *Nat. Chem.* **2010**, *2*, 117.
[47] H. E. Lim, Y. Miyata, R. Kitaura, Y. Nishimura, Y. Nishimoto, S. Irle, J. H. Warner, H. Kataura, H. Shinohara, *Nat. Commun.* **2013**, *4*, 2548.
[48] L. Sun, A. V. Krasheninnikov, T. Ahlgren, K. Nordlund, F. Banhart, *Phys. Rev. Lett.* **2008**, *101*, 156101.
[49] L. Sun, J. Rodriguez-Manzo, F. Banhart, *Appl. Phys. Lett.* **2006**, *89*, 263104.
[50] J. A. Rodríguez-Manzo, C. Pham-Huu, F. Banhart, *ACS Nano* **2011**, *5*, 1529.
[51] Z. Liu, Y.-C. Lin, C.-C. Lu, C.-H. Yeh, P.-W. Chiu, S. Iijima, K. Suenaga, *Nat. Commun.* **2014**, *5*, 4055.

[52] F. Ben Romdhane, T. Björkman, A. V. Krasheninnikov, F. Banhart, *J. Phys. Chem. C* **2014**, *118*, 21001.
[53] F. Ben Romdhane, T. Björkman, J. A. Rodríguez-Manzo, O. Cretu, A. V. Krasheninnikov, F. Banhart, *ACS Nano* **2013**, *7*, 5175.
[54] J. Zhao, Q. Deng, A. Bachmatiuk, G. Sandeep, A. Popov, J. Eckert, M. H. Rümmeli, *Science* **2014**, *343*, 1228.
[55] X. Wei, M.-S. Wang, Y. Bando, D. Golberg, *J. Am. Chem. Soc.* **2010**, *132*, 13592.
[56] X. Wei, M.-S. Wang, Y. Bando, D. Golberg, *ACS Nano* **2011**, *5*, 2916.
[57] I. G. Gonzalez-Martinez, S. M. Gorantla, A. Bachmatiuk, V. Bezugly, J. Zhao, T. Gemming, J. Kunstmann, J. R. Eckert, G. Cuniberti, M. H. Rümmeli, *Nano Lett.* **2014**, *14*, 799.
[58] G. Zhou, L. Luo, L. Li, J. Ciston, E. A. Stach, W. A. Saidi, J. C. Yang, *Chem. Commun.* **2013**, *49*, 10862.
[59] G. Zhou, L. Luo, L. Li, J. Ciston, E. A. Stach, J. C. Yang, *Phys. Rev. Lett.* **2012**, *109*, 235502.
[60] P. L. Hansen, J. B. Wagner, S. Helveg, J. R. Rostrup-Nielsen, B. S. Clausen, H. Topsøe, *Science* **2002**, *295*, 2053.
[61] S. Rackauskas, H. Jiang, J. B. Wagner, S. D. Shandakov, T. W. Hansen, E. I. Kauppinen, A. G. Nasibulin, *Nano Lett.* **2014**, *14*, 5810.
[62] T. Fujita, P. Guan, K. McKenna, X. Lang, A. Hirata, L. Zhang, T. Tokunaga, S. Arai, Y. Yamamoto, N. Tanaka, *Nat. Mater.* **2012**, *11*, 775.
[63] H. Yoshida, Y. Kuwauchi, J. R. Jinschek, K. Sun, S. Tanaka, M. Kohyama, S. Shimada, M. Haruta, S. Takeda, *Science* **2012**, *335*, 317.
[64] H. Xin, S. Alayoglu, R. Tao, A. Genc, C. Wang, L. Kovarik, E. A. Stach, L.-W. Wang, M. Salmeron, G. A. Somorjai, *Nano Lett.* **2014**.
[65] H. L. Xin, E. A. Pach, R. E. Diaz, E. A. Stach, M. Salmeron, H. Zheng, *ACS Nano* **2012**, *6*, 4241.
[66] Y. Kuwauchi, H. Yoshida, T. Akita, M. Haruta, S. Takeda, *Angew. Chem. Int. Ed.* **2012**, *51*, 7729.
[67] J. R. Jinschek, *Chem. Commun.* **2014**, *50*, 2696.
[68] F. M. Ross, in *In-Situ Electron Microscopy* (Eds: G. Dehm, J. M. Howe, J. Zweck), Wiley-VCH, Weinheim, Germany **2012**, Ch. 7.
[69] H. L. Xin, K. Niu, D. H. Alsem, H. Zheng, *Microsc. Microanal.* **2013**, *19*, 1558.
[70] R. Sharma, S.-W. Chee, A. Herzing, R. Miranda, P. Rez, *Nano Lett.* **2011**, *11*, 2464.
[71] S. Hofmann, R. Sharma, C. Ducati, G. Du, C. Mattevi, C. Cepek, M. Cantoro, S. Pisana, A. Parvez, F. Cervantes-Sodi, A. C. Ferrari, R. Dunin-Borkowski, S. Lizzit, L. Petaccia, A. Goldoni, J. Robertson, *Nano Lett.* **2007**, *7*, 602.
[72] M. Lin, J. P. Y. Tan, C. Boothroyd, K. P. Loh, E. S. Tok, Y.-L. Foo, *Nano Lett.* **2007**, *7*, 2234.
[73] J. Huang, S. Chen, Z. Ren, G. Chen, M. Dresselhaus, *Nano Lett.* **2006**, *6*, 1699.
[74] L. He, T. Xu, J. Sun, K. Yin, X. Xie, L. Ding, H. Xiu, L. Sun, *Carbon* **2012**, *50*, 2845.
[75] J. B. Hannon, S. Kodambaka, F. M. Ross, R. M. Tromp, *Nature* **2006**, *440*, 69.
[76] S. Kodambaka, J. B. Hannon, R. M. Tromp, F. M. Ross, *Nano Lett.* **2006**, *6*, 1292.
[77] K. Schwarz, J. Tersoff, S. Kodambaka, Y.-C. Chou, F. Ross, *Phys. Rev. Lett.* **2011**, *107*, 265502.
[78] B. J. Kim, J. Tersoff, S. Kodambaka, J.-S. Jang, E. A. Stach, F. M. Ross, *Nano Lett.* **2014**, *14*, 4554.
[79] K. Schwarz, J. Tersoff, S. Kodambaka, F. Ross, *Phys. Rev. Lett.* **2014**, *113*, 055501.
[80] C. Y. Wen, M. C. Reuter, J. Tersoff, E. A. Stach, F. M. Ross, *Nano Lett.* **2010**, *10*, 514.
[81] C.-Y. Wen, M. C. Reuter, J. Bruley, J. Tersoff, S. Kodambaka, E. A. Stach, F. M. Ross, *Science* **2009**, *326*, 1247.
[82] C.-Y. Wen, J. Tersoff, K. Hillerich, M. Reuter, J. Park, S. Kodambaka, E. Stach, F. Ross, *Phys. Rev. Lett.* **2011**, *107*, 025503.
[83] C.-Y. Wen, J. Tersoff, M. Reuter, E. Stach, F. Ross, *Phys. Rev. Lett.* **2010**, *105*, 195502.
[84] M. Williamson, R. Tromp, P. Vereecken, R. Hull, F. Ross, *Nat. Mater.* **2003**, *2*, 532.
[85] H.-G. Liao, K. Niu, H. Zheng, *Chem. Commun.* **2013**, *49*, 11720.
[86] M. Sun, H.-G. Liao, K. Niu, H. Zheng, *Sci. Rep.* **2013**, *3*, 3227.
[87] N. de Jonge, F. M. Ross, *Nat. Nanotechnol.* **2011**, *6*, 695.
[88] H. L. Xin, H. Zheng, *Nano Lett.* **2012**, *12*, 1470.
[89] K. Jungjohann, S. Bliznakov, P. Sutter, E. A. Stach, E. Sutter, *Nano Lett.* **2013**, *13*, 2964.
[90] K.-Y. Niu, J. Park, H. Zheng, A. P. Alivisatos, *Nano Lett.* **2013**, *13*, 5715.
[91] D. Li, M. H. Nielsen, J. R. Lee, C. Frandsen, J. F. Banfield, J. J. De Yoreo, *Science* **2012**, *336*, 1014.
[92] M. H. Nielsen, S. Aloni, J. J. De Yoreo, *Science* **2014**, *345*, 1158.
[93] Y. Gan, L. Sun, F. Banhart, *Small* **2008**, *4*, 587.
[94] J. A. Rodriguez-Manzo, F. Banhart, *Nano Lett.* **2009**, *9*, 2285.
[95] O. Cretu, A. V. Krasheninnikov, J. A. Rodríguez-Manzo, L. Sun, R. M. Nieminen, F. Banhart, *Phys. Rev. Lett.* **2010**, *105*, 196102.
[96] J. A. Rodríguez-Manzo, O. Cretu, F. Banhart, *ACS Nano* **2010**, *4*, 3422.
[97] H. Qiu, T. Xu, Z. Wang, W. Ren, H. Nan, Z. Ni, Q. Chen, S. Yuan, F. Miao, F. Song, G. Long, Y. Shi, L. Sun, J. Wang, X. Wang, *Nat. Commun.* **2013**, *4*, 2642.
[98] X. Liu, T. Xu, X. Wu, Z. Zhang, J. Yu, H. Qiu, J.-H. Hong, C.-H. Jin, J.-X. Li, X.-R. Wang, L.-T. Sun, W. Guo, *Nat. Commun.* **2013**, *4*, 1776.
[99] J. C. Meyer, F. Eder, S. Kurasch, V. Skakalova, J. Kotakoski, H. J. Park, S. Roth, A. Chuvilin, S. Eyhusen, G. Benner, A. V. Krasheninnikov, U. Kaiser, *Phys. Rev. Lett.* **2012**, *108*, 196102.
[100] N. Wan, J. Xu, T. Xu, M. Matteo, L. Sun, J. Sun, Y. Zhou, *RSC Adv.* **2013**, *3*, 17860.
[101] Z. Yu, Y. Pan, Y. Shen, Z. Wang, Z.-Y. Ong, T. Xu, R. Xin, L. Pan, B. Wang, L. Sun, J. Wang, G. Zhang, Y. W. Zhang, Y. Shi, X. Wang, *Nat. Commun.* **2014**, *5*, 5290.
[102] J. Lin, O. Cretu, W. Zhou, K. Suenaga, D. Prasai, K. I. Bolotin, N. T. Cuong, M. Otani, S. Okada, A. R. Lupini, J.-C. Idrobo, D. Caudel, A. Burger, N. J. Ghimire, J. Yan, D. G. Mandrus, S. J. Pennycook, S. T. Pantelides, *Nat. Nanotechnol.* **2014**, *9*, 436.
[103] C. Jin, H. Lan, L. Peng, K. Suenaga, S. Iijima, *Phys. Rev. Lett.* **2009**, *102*, 205501.
[104] G. Algara-Siller, A. Santana, R. Onions, M. Suyetin, J. Biskupek, E. Bichoutskaia, U. Kaiser, *Carbon* **2013**, *65*, 80.
[105] O. Cretu, A. R. Botello-Mendez, I. Janowska, C. Pham-Huu, J.-C. Charlier, F. Banhart, *Nano Lett.* **2013**, *13*, 3487.
[106] M. Terrones, F. Banhart, N. Grobert, J.-C. Charlier, H. Terrones, P. Ajayan, *Phys. Rev. Lett.* **2002**, *89*, 075505.
[107] M. Terrones, H. Terrones, F. Banhart, J.-C. Charlier, P. Ajayan, *Science* **2000**, *288*, 1226.
[108] J. A. Rodríguez-Manzo, F. Banhart, M. Terrones, H. Terrones, N. Grobert, P. M. Ajayan, B. G. Sumpter, V. Meunier, M. Wang, Y. Bando, D. Golberg, *Proc. Natl. Acad. Sci. USA* **2009**, *106*, 4591.
[109] J. A. Rodríguez-Manzo, M. S. Wang, F. Banhart, Y. Bando, D. Golberg, *Adv. Mater.* **2009**, *21*, 4477.
[110] J. A. Rodriguez-Manzo, A. Tolvanen, A. V. Krasheninnikov, K. Nordlund, A. Demortiere, F. Banhart, *Nanoscale* **2010**, *2*, 901.
[111] J. Li, F. Banhart, *Nano Lett.* **2004**, *4*, 1143.
[112] F. Banhart, J. X. Li, M. Terrones, *Small* **2005**, *1*, 953.
[113] S. Y. Xu, M. L. Tian, J. G. Wang, H. Xu, J. M. Redwing, M. H. W. Chan, *Small* **2005**, *1*, 1221.
[114] T. Xu, X. Xie, L. Sun, in *IEEE NEMS 2013*, IEEE Computer Society, Suzhou, China, **2013**, pp. 637–640.
[115] M. D. Fischbein, M. Drndic, *Nano Lett.* **2007**, *7*, 1329.
[116] T. Xu, X. Xie, K. Yin, J. Sun, L. He, L. Sun, *Small* **2014**, *10*, 1724.

[117] T. Xu, K. Yin, X. Xie, L. He, B. Wang, L. Sun, *Small* **2012**, *8*, 3422.
[118] M. S. Wang, J. Y. Wang, Q. Chen, L. M. Peng, *Adv. Funct. Mater.* **2005**, *15*, 1825.
[119] M. S. Wang, L. M. Peng, J. Y. Wang, Q. Chen, *Adv. Funct. Mater.* **2006**, *16*, 1462.
[120] X. He, T. Xu, X. Xu, Y. Zeng, J. Xu, L. Sun, C. Wang, H. Xing, B. Wu, A. Lu, D. Liu, X. Chen, J. Chu, *Sci. Rep.* **2014**, *4*, 6544.
[121] Y. Khalavka, C. Ohm, L. Sun, F. Banhart, C. Sönnichsen, *J. Phys. Chem. C* **2007**, *111*, 12886.
[122] V. C. Holmberg, M. G. Panthani, B. A. Korgel, *Science* **2009**, *326*, 405.
[123] R. Zou, Z. Zhang, Q. Tian, G. Ma, G. Song, Z. Chen, J. Hu, *Small* **2011**, *7*, 3377.
[124] Y. Ding, F. Fan, Z. Tian, Z. L. Wang, *Small* **2009**, *5*, 2812.
[125] B. Goris, M. A. Van Huis, S. Bals, H. W. Zandbergen, L. Manna, G. Van Tendeloo, *Small* **2012**, *8*, 937.
[126] X. Jia, M. Hofmann, V. Meunier, B. G. Sumpter, J. Campos-Delgado, J. M. Romo-Herrera, H. Son, Y.-P. Hsieh, A. Reina, J. Kong, M. Terrones, M. S. Dresselhaus, *Science* **2009**, *323*, 1701.
[127] K. Kim, W. Regan, B. Geng, B. Alemán, B. M. Kessler, F. Wang, M. F. Crommie, A. Zettl, *Phys.Status Solidi RRL* **2010**, *4*, 302.
[128] J. Y. Huang, S. Chen, Z. Q. Wang, K. Kempa, Y. M. Wang, S. H. Jo, G. Chen, M. S. Dresselhaus, Z. F. Ren, *Nature* **2006**, *439*, 281.
[129] N. Wan, L. Sun, S. Ding, T. Xu, X. Hu, J. Sun, H. Bi, *Carbon* **2013**, *53*, 260.
[130] J. Y. Huang, F. Ding, B. I. Yakobson, P. Lu, L. Qi, J. Li, *Proc. Natl. Acad. Sci. USA* **2009**, *106*, 10103.
[131] N. Wan, P. Perriat, L.-T. Sun, Q.-A. Huang, J. Sun, T. Xu, *Appl. Phys. Lett.* **2012**, *100*, 193111.
[132] B. Regan, S. Aloni, R. Ritchie, U. Dahmen, A. Zettl, *Nature* **2004**, *428*, 924.
[133] K. Svensson, H. Olin, E. Olsson, *Phys. Rev. Lett.* **2004**, *93*, 145901.
[134] D. Golberg, P. M. Costa, M. Mitome, S. Hampel, D. Haase, C. Mueller, A. Leonhardt, Y. Bando, *Adv. Mater.* **2007**, *19*, 1937.
[135] P. M. Costa, D. Golberg, M. Mitome, S. Hampel, A. Leonhardt, B. Buchner, Y. Bando, *Nano Lett.* **2008**, *8*, 3120.
[136] L. Dong, X. Tao, M. Hamdi, L. Zhang, X. Zhang, A. Ferreira, B. J. Nelson, *Nano Lett.* **2008**, *9*, 210.
[137] S. Mei, L. He, X. Wu, J. Sun, B. Wang, X. Xiong, L. Sun, *Nanoscale* **2014**, *6*, 405.
[138] M. Löffler, U. Weissker, T. Mühl, T. Gemming, J. Eckert, B. Büchner, *Adv. Mater.* **2011**, *23*, 541.
[139] S. Coh, W. Gannett, A. Zettl, M. L. Cohen, S. G. Louie, *Phys. Rev. Lett.* **2013**, *110*, 185901.
[140] A. Barreiro, R. Rurali, E. R. Hernandez, J. Moser, T. Pichler, L. Forro, A. Bachtold, *Science* **2008**, *320*, 775.
[141] R. Spolenak, in *In-Situ Electron Microscopy* (Eds: G. Dehm, J. M. Howe, J. Zweck), Wiley-VCH, Weinheim, Germany **2012**, Ch. 12.
[142] J. Zhao, J.-Q. Huang, F. Wei, J. Zhu, *Nano Lett.* **2010**, *10*, 4309.
[143] J. W. Wang, S. Narayanan, J. Y. Huang, Z. Zhang, T. Zhu, S. X. Mao, *Nat. Commun.* **2013**, *4*, 2340.
[144] J. Wang, F. Sansoz, J. Huang, Y. Liu, S. Sun, Z. Zhang, S. X. Mao, *Nat. Commun.* **2013**, *4*, 1742.
[145] J. Y. Huang, H. Zheng, S. Mao, Q. Li, G. T. Wang, *Nano Lett.* **2011**, *11*, 1618.
[146] H. Zheng, A. Cao, C. R. Weinberger, J. Y. Huang, K. Du, J. Wang, Y. Ma, Y. Xia, S. X. Mao, *Nat. Commun.* **2010**, *1*, 144.
[147] J. Sun, L. He, Y.-C. Lo, T. Xu, H. Bi, L. Sun, Z. Zhang, S. X. Mao, J. Li, *Nat. Mater.* **2014**, *13*, 1007.
[148] Y. Lu, J. Y. Huang, C. Wang, S. Sun, J. Lou, *Nat. Nanotechnol.* **2010**, *5*, 218.
[149] K. Zheng, C. Wang, Y.-Q. Cheng, Y. Yue, X. Han, Z. Zhang, Z. Shan, S. X. Mao, M. Ye, Y. Yin, E. Ma, *Nat. Commun.* **2010**, *1*, 24.
[150] K. Zheng, X. Han, L. Wang, Y. Zhang, Y. Yue, Y. Qin, X. Zhang, Z. Zhang, *Nano Lett.* **2009**, *9*, 2471.
[151] X. Han, K. Zheng, Y. Zhang, X. Zhang, Z. Zhang, Z. L. Wang, *Adv. Mater.* **2007**, *19*, 2112.
[152] X. Han, Y. Zhang, K. Zheng, X. Zhang, Z. Zhang, Y. Hao, X. Guo, J. Yuan, Z. Wang, *Nano Lett.* **2007**, *7*, 452.
[153] L. Wang, P. Liu, P. Guan, M. Yang, J. Sun, Y. Cheng, A. Hirata, Z. Zhang, E. Ma, M. Chen, *Nat. Commun.* **2013**, *4*, 2413.
[154] L. Wang, K. Zheng, Z. Zhang, X. Han, *Nano Lett.* **2011**, *11*, 2382.
[155] M. S. Wang, D. Golberg, Y. Bando, *Adv. Mater.* **2010**, *22*, 4071.
[156] X. Wei, M. S. Wang, Y. Bando, D. Golberg, *Adv. Mater.* **2010**, *22*, 4895.
[157] D.-M. Tang, X. Wei, M.-S. Wang, N. Kawamoto, Y. Bando, C. Zhi, M. Mitome, A. Zak, R. Tenne, D. Golberg, *Nano Lett.* **2013**, *13*, 1034.
[158] H. D. Espinosa, R. A. Bernal, T. Filleter, *Small* **2012**, *8*, 3233.
[159] D.-M. Tang, C.-L. Ren, M.-S. Wang, X. Wei, N. Kawamoto, C. Liu, Y. Bando, M. Mitome, N. Fukata, D. Golberg, *Nano Lett.* **2012**, *12*, 1898.
[160] D.-M. Tang, D. G. Kvashnin, S. Najmaei, Y. Bando, K. Kimoto, P. Koskinen, P. M. Ajayan, B. I. Yakobson, P. B. Sorokin, J. Lou, D. Golberg, *Nat. Commun.* **2014**, *5*, 3631.
[161] D. Golberg, P. M. F. J. Costa, M.-S. Wang, X. Wei, D.-M. Tang, Z. Xu, Y. Huang, U. K. Gautam, B. Liu, H. Zeng, N. Kawamoto, C. Zhi, M. Mitome, Y. Bando, *Adv. Mater.* **2012**, *24*, 177.
[162] I. Nikiforov, D.-M. Tang, X. Wei, T. Dumitrica, D. Golberg, *Phys. Rev. Lett.* **2012**, *109*, 025504.
[163] Z. Shan, G. Adesso, A. Cabot, M. Sherburne, S. S. Asif, O. Warren, D. Chrzan, A. Minor, A. Alivisatos, *Nat. Mater.* **2008**, *7*, 947.
[164] Z. Shan, R. K. Mishra, S. S. Asif, O. L. Warren, A. M. Minor, *Nat. Mater.* **2008**, *7*, 115.
[165] Q. Yu, Z.-W. Shan, J. Li, X. Huang, L. Xiao, J. Sun, E. Ma, *Nature* **2010**, *463*, 335.
[166] D. Kiener, P. Hosemann, S. Maloy, A. Minor, *Nat. Mater.* **2011**, *10*, 608.
[167] L. Huang, Q.-J. Li, Z.-W. Shan, J. Li, J. Sun, E. Ma, *Nat. Commun.* **2011**, *2*, 547.
[168] B. Peng, M. Locascio, P. Zapol, S. Li, S. L. Mielke, G. C. Schatz, H. D. Espinosa, *Nat. Nanotechnol.* **2008**, *3*, 626.
[169] J. Sun, F. Xu, L.-T. Sun, *Acta Mech. Sinica* **2012**, *28*, 1513.
[170] G. Dehm, M. Legros, D. Kiener, in *In-Situ Electron Microscopy* (Eds: G. Dehm, J. M. Howe, J. Zweck), Wiley-VCH, Weinheim, Germany **2012**, Ch. 10.
[171] A. M. Minor, in *In-Situ Electron Microscopy* (Eds: G. Dehm, J. M. Howe, J. Zweck), Wiley-VCH, Weinheim, Germany **2012**, Ch. 11.
[172] L. Wang, Z. Zhang, X. Han, *NPG Asia Mater.* **2013**, *5*, e40.
[173] S. Yang, L. Wang, X. Tian, Z. Xu, W. Wang, X. Bai, E. Wang, *Adv. Mater.* **2012**, *24*, 4676.
[174] F. Cavalca, A. B. Laursen, B. E. Kardynal, R. E. Dunin-Borkowski, S. Dahl, J. B. Wagner, T. W. Hansen, *Nanotechnology* **2012**, *23*, 075705.
[175] L. Zhang, B. K. Miller, P. A. Crozier, *Nano Lett.* **2013**, *13*, 679.
[176] J. Zweck, in *In-Situ Electron Microscopy* (Eds: G. Dehm, J. M. Howe, J. Zweck), Wiley-VCH, Weinheim, Germany **2012**, Ch. 15.
[177] E. Snoeck, C. Gatel, in *Transmission Electron Microscopy in Micro-Nanoelectronics*, Wiley-ISTE, Hoboken, USA **2013**, Ch. 5.
[178] J. Li, F. Banhart, *Adv. Mater.* **2005**, *17*, 1539.
[179] J. Sun, Q. Liu, H. Xie, X. Wu, F. Xu, T. Xu, S. Long, H. Lv, Y. Li, L. Sun, M. Liu, *Appl. Phys. Lett.* **2013**, *102*, 053502.
[180] Y. Yang, P. Gao, S. Gaba, T. Chang, X. Pan, W. Lu, *Nat. Commun.* **2012**, *3*, 732.
[181] Y. Yang, W. Lu, Y. Yao, J. Sun, C. Gu, L. Gu, Y. Wang, X. Duan, R. Yu, *Sci. Rep.* **2014**, *4*, 3890.
[182] X. Tian, S. Yang, M. Zeng, L. Wang, J. Wei, Z. Xu, W. Wang, X. Bai, *Adv. Mater.* **2014**, *26*, 3649.

[183] J.-Y. Chen, C.-L. Hsin, C.-W. Huang, C.-H. Chiu, Y.-T. Huang, S.-J. Lin, W.-W. Wu, L.-J. Chen, *Nano Lett.* **2013**, *13*, 3671.
[184] D.-H. Kwon, K. M. Kim, J. H. Jang, J. M. Jeon, M. H. Lee, G. H. Kim, X.-S. Li, G.-S. Park, B. Lee, S. Han, M. Kim, C. S. Hwang, *Nat. Nanotechnol.* **2010**, *5*, 148.
[185] Y. Yang, P. Gao, L. Li, X. Pan, S. Tappertzhofen, S. Choi, R. Waser, I. Valov, W. D. Lu, *Nat. Commun.* **2014**, *5*, 4232.
[186] H. Xu, Y. Xia, K. Yin, J. Lu, Q. Yin, J. Yin, L. Sun, Z. Liu, *Sci. Rep.* **2013**, *3*, 1230.
[187] X. H. Liu, J. Y. Huang, *Energy Environ. Sci.* **2011**, *4*, 3844.
[188] X. H. Liu, Y. Liu, A. Kushima, S. Zhang, T. Zhu, J. Li, J. Y. Huang, *Adv. Energy Mater.* **2012**, *2*, 722.
[189] A. Kushima, X. H. Liu, G. Zhu, Z. L. Wang, J. Y. Huang, J. Li, *Nano Lett.* **2011**, *11*, 4535.
[190] X. H. Liu, L. Q. Zhang, L. Zhong, Y. Liu, H. Zheng, J. W. Wang, J.-H. Cho, S. A. Dayeh, S. T. Picraux, J. P. Sullivan, *Nano Lett.* **2011**, *11*, 2251.
[191] C.-M. Wang, W. Xu, J. Liu, J.-G. Zhang, L. V. Saraf, B. W. Arey, D. Choi, Z.-G. Yang, J. Xiao, S. Thevuthasan, *Nano Lett.* **2011**, *11*, 1874.
[192] L. Q. Zhang, X. H. Liu, Y. Liu, S. Huang, T. Zhu, L. Gui, S. X. Mao, Z. Z. Ye, C. M. Wang, J. P. Sullivan, *ACS Nano* **2011**, *5*, 4800.
[193] L. Zhong, X. H. Liu, G. F. Wang, S. X. Mao, J. Y. Huang, *Phys. Rev. Lett.* **2011**, *106*, 248302.
[194] C.-M. Wang, X. Li, Z. Wang, W. Xu, J. Liu, F. Gao, L. Kovarik, J.-G. Zhang, J. Howe, D. J. Burton, Z. Liu, X. Xiao, S. Thevuthasan, D. R. Baer, *Nano Lett.* **2012**, *12*, 1624.
[195] M. Gu, L. R. Parent, B. L. Mehdi, R. R. Unocic, M. T. McDowell, R. L. Sacci, W. Xu, J. G. Connell, P. Xu, P. Abellan, X. Chen, Y. Zhang, D. E. Perea, J. E. Evans, L. J. Lauhon, J.-G. Zhang, J. Liu, N. D. Browning, Y. Cui, I. Arslan, C.-M. Wang, *Nano Lett.* **2013**, *13*, 6106.
[196] M. E. Holtz, Y. Yu, D. Gunceler, J. Gao, R. Sundararaman, K. A. Schwarz, T. A. Arias, H. D. Abruña, D. A. Muller, *Nano Lett.* **2014**, *14*, 1453.
[197] X. H. Liu, H. Zheng, L. Zhong, S. Huang, K. Karki, L. Q. Zhang, Y. Liu, A. Kushima, W. T. Liang, J. W. Wang, J.-H. Cho, E. Epstein, S. A. Dayeh, S. T. Picraux, T. Zhu, J. Li, J. P. Sullivan, J. Cumings, C. Wang, S. X. Mao, Z. Z. Ye, S. Zhang, J. Y. Huang, *Nano Lett.* **2011**, *11*, 3312.
[198] X. H. Liu, S. Huang, S. T. Picraux, J. Li, T. Zhu, J. Y. Huang, *Nano Lett.* **2011**, *11*, 3991.
[199] Y. Liu, N. S. Hudak, D. L. Huber, S. J. Limmer, J. P. Sullivan, J. Y. Huang, *Nano Lett.* **2011**, *11*, 4188.
[200] Y. Liu, H. Zheng, X. H. Liu, S. Huang, T. Zhu, J. Wang, A. Kushima, N. S. Hudak, X. Huang, S. Zhang, S. X. Mao, X. Qian, J. Li, J. Y. Huang, *ACS Nano* **2011**, *5*, 7245.
[201] X. H. Liu, F. Fan, H. Yang, S. Zhang, J. Y. Huang, T. Zhu, *ACS Nano* **2012**, *7*, 1495.
[202] X. H. Liu, J. W. Wang, S. Huang, F. Fan, X. Huang, Y. Liu, S. Krylyuk, J. Yoo, S. A. Dayeh, A. V. Davydov, *Nat. Nanotechnol.* **2012**, *7*, 749.
[203] X. H. Liu, J. W. Wang, Y. Liu, H. Zheng, A. Kushima, S. Huang, T. Zhu, S. X. Mao, J. Li, S. Zhang, W. Lu, J. M. Tour, J. Y. Huang, *Carbon* **2012**, *50*, 3836.
[204] X. H. Liu, L. Zhong, S. Huang, S. X. Mao, T. Zhu, J. Y. Huang, *ACS Nano* **2012**, *6*, 1522.
[205] J. W. Wang, X. H. Liu, K. Zhao, A. Palmer, E. Patten, D. Burton, S. X. Mao, Z. Suo, J. Y. Huang, *ACS Nano* **2012**, *6*, 9158.
[206] W. Liang, L. Hong, H. Yang, F. Fan, Y. Liu, H. Li, J. Li, J. Y. Huang, L.-Q. Chen, T. Zhu, *Nano Lett.* **2013**, *13*, 5212.
[207] W. Liang, H. Yang, F. Fan, Y. Liu, X. H. Liu, J. Y. Huang, T. Zhu, S. Zhang, *ACS Nano* **2013**, *7*, 3427.
[208] J. W. Wang, Y. He, F. Fan, X. H. Liu, S. Xia, Y. Liu, C. T. Harris, H. Li, J. Y. Huang, S. X. Mao, T. Zhu, *Nano Lett.* **2013**, *13*, 709.
[209] L. Zhong, R. R. Mitchell, Y. Liu, B. M. Gallant, C. V. Thompson, J. Y. Huang, S. X. Mao, Y. Shao-Horn, *Nano Lett.* **2013**, *13*, 2209.
[210] Y. Zhu, J. W. Wang, Y. Liu, X. Liu, A. Kushima, Y. Liu, Y. Xu, S. X. Mao, J. Li, C. Wang, J. Y. Huang, *Adv. Mater.* **2013**, *25*, 5461.
[211] J. Niu, A. Kushima, X. Qian, L. Qi, K. Xiang, Y.-M. Chiang, J. Li, *Nano Lett.* **2014**, *14*, 4005.
[212] K. Yamamoto, Y. Iriyama, T. Asaka, T. Hirayama, H. Fujita, C. A. J. Fisher, K. Nonaka, Y. Sugita, Z. Ogumi, *Angew. Chem.* **2010**, *122*, 4516.
[213] J. W. Wang, X. H. Liu, S. X. Mao, J. Y. Huang, *Nano Lett.* **2012**, *12*, 5897.
[214] M. Gu, A. Kushima, Y. Shao, J.-G. Zhang, J. Liu, N. D. Browning, J. Li, C. Wang, *Nano Lett.* **2013**, *13*, 5203.
[215] X. Han, Y. Liu, Z. Jia, Y.-C. Chen, J. Wan, N. Weadock, K. J. Gaskell, T. Li, L. Hu, *Nano Lett.* **2013**, *14*, 139.
[216] K. He, Y. Zhou, P. Gao, L. Wang, N. Pereira, G. G. Amatucci, K.-W. Nam, X.-Q. Yang, Y. Zhu, F. Wang, D. Su, *ACS Nano* **2014**, *8*, 7251.
[217] Y. Liu, F. Fan, J. Wang, Y. Liu, H. Chen, K. L. Jungjohann, Y. Xu, Y. Zhu, D. Bigio, T. Zhu, C. Wang, *Nano Lett.* **2014**, *14*, 3445.
[218] E. S. Hall, H. Zheng, Y. Zhu, in *Report of the Basic Energy Sciences Workshop on Future of Electron Scattering and Diffraction*, US Department of Energy, Washington, DC **2014**, available at http://science.energy.gov/bes/news-and-resources/reports/.

Received: November 1, 2014
Revised: December 13, 2014
Published online: February 19, 2015